Simulation of Droplet Impact and Spreading using a Simple Dynamic Contact Angle Model

S. G. Mallinson[1,2], **T. J. Barber**[2], **G. H. Yeoh**[2] **and G. D. McBain**[1]

[1]Memjet
Macquarie Park, New South Wales, 2113, Australia

[2]School of Mechanical and Manufacturing Engineering
University of New South Wales, Kensington, New South Wales 2052, Australia

Abstract

Numerical simulations of droplet impact have been performed using a two-phase VOF-based solver. Comparison with experimental data for droplet shape, maximum diameter and minimum height is reasonable. Simulation results for maximum droplet diameter, for a range of conditions pertinent to inkjet printing, have been compared with several empirical correlations; none of the correlations capture all of the results particularly well.

Introduction

The impact and subsequent spreading of a droplet on a solid surface is encountered in many situations of practical importance, for example, inkjet printing, 3D additive manufacturing and spray coating.

The amount of areal coverage provided by a single droplet is an important factor in these industrial settings: it is commonly characterised by the ratio of the maximum dot diameter to the initial droplet diameter, D^*, often called the spreading or splat factor.
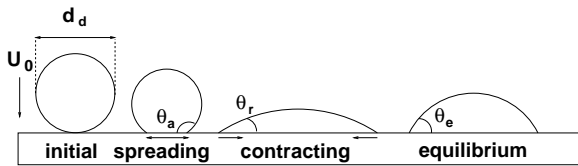

Figure 1: Schematic showing contact angle definitions.

Droplet Spreading Factor

Several researchers have examined how D^* varies with droplet properties, and the resulting values have been correlated in terms of the Reynolds and Weber numbers, Re and We, respectively:

$$Re = \frac{\rho_d U_0 d_d}{\mu_d} \tag{1}$$

$$We = \frac{\rho_d U_0^2 d_d}{\sigma_d} \tag{2}$$

Here, ρ is density, U_0 is initial droplet velocity, d is diameter, μ is viscosity, σ is surface tension and the subscript 'd' refers to droplet properties.

Asai et al [1] correlated their experimental data for D^* in the form:

$$D^* = 1 + aWe^{0.5} \exp\left(-bWe^c Re^{-d}\right) \tag{3}$$

where $a = 0.48$, $b = 1.48$, $c = 0.22$ and $d = 0.21$. Toivakka [19] fit results from numerical simulations in a similar form with $a = 13.51$, $b = 4.28$, $c = 0.072$ and $d = 0.043$. Bayer and

Megaridis [2] and Scheller and Bousfield [18] proposed correlating data using:

$$D^* = e\left(ReWe^{1/2}\right)^f \tag{4}$$

where $e = 0.72$ and $f = 0.14$ for the former and $e = 0.61$ and $f = 0.166$ for the latter. Roisman [17] presented a two-parameter correlation of experimental data with the terms coming from an analysis of different flow regimes:

$$D^* = gRe^{0.2} - h\frac{Re^{0.4}}{\sqrt{We}} \tag{5}$$

with $g = 0.87$ and $h = 0.47$. Feng [7] found $g = 1.0$ and $h = 0.35$ provided a better fit to his simulation predictions.

None of these expressions included the effect of the contact angle. Pasandideh-Fard et al [16] proposed the following expression, based on conservation of energy and an assumption of axisymmetric stagnation point flow in the liquid:

$$D^* = \sqrt{\frac{We + 12}{3\left(1 - \cos\theta_a\right) + 4\left(We/\sqrt{Re}\right)}} \tag{6}$$

Feng suggested multiplying equations 5 and 6 together to provide better estimates of simulated spread factors than either equation by itself.

Empirical correlations can provide design estimates of D^* for the range of parameters from which they were developed. Each droplet deposition system will have its own characteristics, often outside the parameter values used in the correlation. Numerical simulation allows the designer to estimate D^* for all parameter values. Some earlier numerical investigations of droplet impact and spread are presented and discussed below.

Most numerical investigations of droplet impact and spreading have used the volume-of-fluid (VOF) method [10] and some kind of model for the dynamic variation of contact angle with interface velocity. The models normally define a dynamic angle, θ_d, as a function of some combination of the equilbrium, advancing and receding angles, θ_e, θ_a and θ_r, respectively; see figure 1 which shows how these angles are defined.

Pasandideh-Fard et al [16] used a finite-difference Navier–Stokes solver together with a VOF model, to simulate their experiments for a droplet with $Re = 2000$, $We = 27.8$. They found the numerical results which used the measured contact angle as a function of interface velocity to agree better with the data than a calculation which assumed the contact angle to be constant, equal to the equilibrium contact angle. Toivakka [19] used a finite-volume VOF-based solver to compute droplet spread, and assumed a constant, equilibrium contact angle. The main focus in that paper was the impact of shear-thinning rheology, and paper motion. Yokoi et al [21] used a finite-volume code together

with a coupled level set / VOF model to simulate droplet impact with $Re = 2280$ and $We = 32$. They combined a simple switching model:

$$\theta_d = \begin{cases} \theta_a, & \text{if } U_w \geq 0 \\ \theta_r, & \text{if } U_w < 0 \end{cases} \qquad (7)$$

where U_w is the velocity near the wall, normal to the interface, together with the Voinov–Cox [20, 5] model, derived from lubrication theory:

$$\theta_d^3 = \theta_e^3 + kCa \qquad (8)$$

where $Ca = \mu U / \sigma$ is the capillary number, the parameter $k = 72$ [12]. Gujjula [9] compared the data of Pasandideh-Fard et al with results from a finite-volume solver using a VOF model together with a number of different dynamic contact angle models: Voinov–Cox, equation 8, Jiang et al [13] and Bracke et al [4]. The second and third models are empirical fits to experimental data:

$$\cos\theta_d = \cos\theta_e - 2\left(1 + \cos\theta_e\right)\sqrt{Ca} \qquad (9)$$

and,

$$\cos\theta_d = \cos\theta_e - \left(1 + \cos\theta_e\right)\tanh 4.96 Ca^{0.702} \qquad (10)$$

respectively. Gujjula found these models to underpredict the measured spread with time. Feng [7] used finite-volume / VOF simulations together with the dynamic contact angle model implemented in the OpenFOAM library:

$$\theta = \theta_e + (\theta_a - \theta_r)\tanh\left(\frac{U_w}{U_\theta}\right) \qquad (11)$$

where and U_θ is a characteristic velocity scale. Feng assumed $\theta_a = 95°$, $\theta_r = 85°$, and $\theta_e = 90°$. The simulations results compared well with empirical correlations.

All of the above investigations considered axisymmetric flow domains. Fujimoto et al [8] compared experimental data for $Re = 1570$ and $We = 56$ with result from a three-dimensional finite-difference solver with a VOF model, assuming a simple switching dynamic contact angle model, equation 7. They obtained very good agreement between simulation and experiment for a range of different impact angles.

Inspection of the abovementioned dynamic contact models indicates issues with some of them. For equations 8, 9 and 10, the expressions are invalid for values of Ca near to or just less than zero; that is during the region applicable to droplet retraction. Equation 11 has asymptotic values of $\theta_e \pm (\theta_a - \theta_r)$, which could lead to unphysical values if the second term is greater than the first. The one model which gives reasonable values for all Ca is the switching model, equation 7.

Summary of Paper

Here, we have conducted numerical simulations using the two-phase flow solver *interFoam* [15, 6], part of the OpenFOAM library. The dynamic contact angle is modelled using a simple switching condition:

$$\theta_d = \begin{cases} \theta_a, & \text{if } U_w > 0 \\ \theta_e, & \text{if } U_w = 0 \\ \theta_r, & \text{if } U_w < 0 \end{cases} \qquad (12)$$

We have chosen to slightly modify the switching model from the one used by Fujimoto [8] et al to permit the free-surface to adopt the equilibrium angle in contact with the solid when motion ceases. The method is compared against the experimental data of Fujimoto et al for a $d_d = 0.56$ mm diameter

droplet impacting a solid surface normally with a velocity of $U_0 = 2.7$ m s^{-1}. A series of simulations are then performed for a range of Re and We of interest to inkjet printer designers, and the values of the maximum spreading factor are compared with empirical correlations.

Numerical Methods

Governing Equations

In the *interFoam* solver, the continuity and Navier–Stokes equations, equations 13 and 14, respectively, are solved together with a transport equation for the volume-fraction of liquid, α, equation 15 [10].

$$\nabla \cdot \mathbf{U} = 0 \qquad (13)$$

$$\rho\frac{D\mathbf{U}}{Dt} = -\nabla p + \rho g + \nabla \cdot \mu\left(\nabla\mathbf{U} + \nabla\mathbf{U}^T\right) + \mathbf{F}_\sigma \qquad (14)$$

$$\frac{D\alpha}{Dt} = 0 \qquad (15)$$

Here $\mathbf{U}$ = velocity-vector, t = time, p = pressure, g = gravitational acceleration, and $\mathbf{F}_\sigma$ = surface tension body forces.

The fluid properties are calculated as the volume fraction weighted-average:

$$\rho = \alpha\rho_l + (1-\alpha)\rho_g \qquad (16)$$

$$\mu = \alpha\mu_l + (1-\alpha)\mu_g \qquad (17)$$

where α is one in the liquid phase, zero in the gas phase and takes intermediate values near the interface; the subscripts 'l' and 'g' refer to the liquid and gas phases respectively.

The surface tension body force is modelled using the continuum surface force method [3]:

$$\mathbf{F}_\sigma = \sigma k\mathbf{n} \qquad (18)$$

where σ = liquid-gas surface tension coefficient, $k = \nabla \cdot \mathbf{n}$ = interfacial curvature and $\mathbf{n} = \nabla\alpha/|\nabla\alpha|$ is the interfacial norm, which only takes non-zero values at the interface.

The interface between the phases is typically smeared over several cells in the standard VOF method. To provide sharper interfaces, *interFoam* adds an additional compression term to the LHS of Equation 15: $-\nabla[\alpha(1-\alpha)\mathbf{U}_r]$. The artificial compression velocity is given by:

$$\mathbf{U}_r = \mathbf{n}_f \min\left[C_\gamma\frac{|\phi|}{|S_f|}, \max\left(\frac{|\phi|}{|S_f|}\right)\right] \qquad (19)$$

where $\mathbf{n}_f$ is the vector normal to the cell surface, ϕ is the mass flux and S_f is the cell surface area. The compression coefficient, C_γ, sets the level of compression; if it is equal to zero, there is no compression, whilst setting it to one gives a balance between interface compression and unwanted parasitic currents [6, 11]. Here, we have used $C_\gamma = 1$.

The transient terms are solved using Crank–Nicolson time-stepping, and the time step is set using a maximum Courant number of 0.2. The spatial terms are discretized using second-order centred-differencing. Pressure coupling is achieved using

the PISO method. The pressure equation is solved using the diagonal incomplete-Cholesky preconditioned conjugate gradient method. The velocity and VOF equations are solved using the symmetric Gauss–Seidel method; the interface compression term is solved using the MULES technique [15].

For the initial calculations, the computational domain was similar to that used by Fujimoto et al [8]: a half-domain ($3d_p \times 1.5d_p \times 1.5d_p$) with symmetry at $y = 0$. The number of cells in the x- and y-directions are 160×80, with a uniform cell-size. In the z-direction, 128 cells are used, and stretching is applied from the wall outwards, with a total stretching factor of approximately 4.34. In later simulations of droplets with properties of interest to inkjet printing, we use the same mesh, scaled to the initial droplet size.

At the wall, no slip conditions are applied to velocity, together with zero gradient for pressure, which includes a correction for surface tension terms. The boundary conditions on the volume fraction are set using the simple switching dynamic contact angle model, equation 12. This required two minor modifications to the existing dynamic contact angle model in OpenFOAM: (i) change the sign of the computed wall velocity, so that flow towards the lighter phase is positive, and thus contact angles are defined as in figure 1; and, (ii) modify the returned value:

```
return theta0_
        + (thetaA_ - theta0_) * pos(uwall)
        + (thetaR_ - theta0_) * neg(uwall);
```

At the top and side boundaries, the pressure is held constant during outflow, whilst the total pressure is constant during inflow. At these boundaries, zero gradient conditions are applied to the normal velocity, with the tangential velocity set to zero.

Fujimoto et al specified the air and water density as 1.2 kg m^{-3} and 1000 kg m^{-3}, respectively. Given values of Re and We, we can deduce values for the water viscosity and surface tension. The viscosity of air is estimated from Sutherland's law at $25°C$ to be $18.41 \, \mu\text{Pa s}$. Consistent with the original paper, we have included the effects of gravity, even though the value of the Bond number is much less than unity.

Results

Comparison with Experimental Data

The simulated droplet shape is compared with experimental droplet visualization data in figure 2. Overall, the comparison is fair, although there are some details which are not faithfully captured; for example, the predicted height in the second instant is lower than the measured value.

A more quantitative comparison is presented in figure 3, which compares the normalized droplet diameter and height as a function of time for the earlier experiments and simulations (on the finest mesh) with the present simulations at three different resulutions. Overall the comparison between the current numerical predictions and the data is reasonable, but not as good as the Fujimoto et al simulation. For example, the difference between the experimental and numerical peak value of D^* is less than 1% for the Fujimoto et al simulations, and approximately 2% for the current computations.

Effect of Reynolds and Weber Numbers in Memjet Systems

Memjet have developed a variety of inkjet platforms which produce droplets with diameter, velocity and material properties such that $15 \leq Re \leq 240$ and $8 \leq We \leq 392$. Thus it was decided to perform a matrix of simulations with $Re = (15, 60, 240)$ and
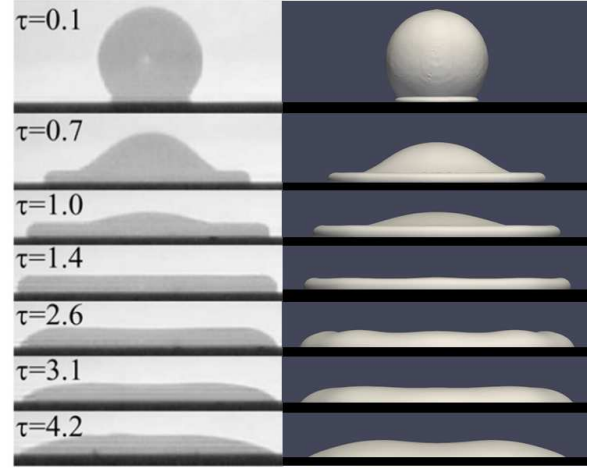

Figure 2: Comparison of experimental droplet visualization (left) with current numerical predictions (right).
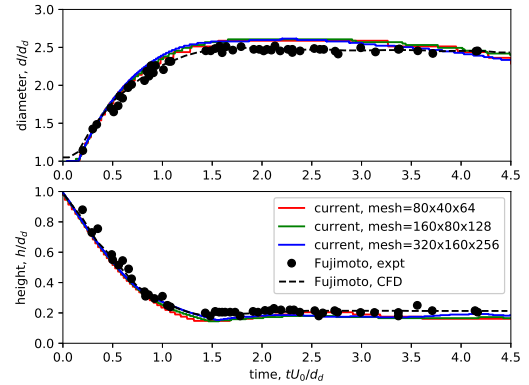

Figure 3: Normalized diameter and height as a function of time.

$We = (8, 56, 392)$. We assumed contact angles typical of ink formulations on a highly wettable surface: $\theta_a = 60°$, $\theta_r = 5°$, and $\theta_e = 10°$. The normalized values of maximum diameter and minimum height, D^* and H^*, are presented in table 1 for the matrix of simulation cases.

Table 2 compares the average difference between the simulation results and each of the theoretical correlations presented in the Introducton. None of the correlations is able to capture all of the data very well, although the ones from [1, 19, 7] seem to perform a little better than the others.

Discussion and Conclusions

The comparison between the current simulation model and the data of Fujimoto et al [8] shows very little difference between the results obtained on three successively refined meshes: the maximum values of D^* were 2.59, 2.61 and 2.62 for $80 \times 40 \times 64$, $160 \times 80 \times 128$ and $320 \times 160 \times 256$ meshes, respectively.

Empirical correlations did not seem to provide good estimates of the droplet spread factor from simulations. It is possible, however, to vary the fitting parameters to provide a better fit. For example, considering equation 3, the four fitting parameters can be optimized: a = 1.672, b = 1.342, c = 0.1544 and d = 0.02362. Using equation 3 with these parameters gives an average error of approximately 4%, compared with approxi-

Re	We	D*	H*
15	8	1.78	0.29
15	56	2.08	0.18
15	392	2.46	0.13
60	8	1.89	0.27
60	56	2.04	0.19
60	392	2.38	0.13
240	8	2.16	0.11
240	56	2.42	0.15
240	392	2.71	0.11

Table 1: Summary of resulta of simulations of droplet impact for a range of parameters of interest.

Ref.	Difference (%)
[1]	28
[19]	20
[2]	30
[18]	32
[17]	51
[7]	18
[16]	48
[7] & [16]	37

Table 2: Comparison average difference between values of D^* for current simulation and empirical correlations from different investigators.

mately 28% for the original parameters.

The numerical simulations using a simple switching dynamic contact angle model, equation 12, are in good agreement with experimental data, and allow the inkjet printer designer to estimate spread factors for the various different droplet properties considered here.

Acknowledgements

References

[1] Asai, A., Shioya, M., Hirasawa, S. and Okazaki, T., Impact of an Ink Drop on Paper, *J. Imaging Sci. Tech.*, **37**, 1993, pp. 205–207.

[2] Bayer, I.S. and Megaridis, C.M., Contact Angle Dynamics in Droplets Impacting on Flat Surfaces with Different Wetting Characteristics, *J. Fluid Mech.*, **558**, 2006, pp. 415–449.

[3] Brackbill, J.U., Kothe D.B. and Zemach, C., A Continuum Method for Modeling Surface Tension, *J. Comp. Phys.*, **100**, 1992, pp. 335–354.

[4] Bracke, M., De Voeght, F. and Joos, P., The Kinetics of Wetting: The Dynamic Contact Angle, *Progr. Colloid Polym. Sci.*, **79**, 1989, pp 142–149.

[5] Cox, R.G., The Dynamics of the Spreading of Liquids on a Solid Surface. Part 1. Viscous Flow, *J. Fluid Mech.*, **168**, 1986, pp 169–194.

[6] Deshpande, S.S., Anumolu, L. and Trujillo, M.F., Evaluating the Performance of the Two–Phase Flow Solver interFoam, *Comp. Sci. Disc.*, **5**, 2012, p. 014016.

[7] Feng, J.Q., A Computational Study of High–Speed Microdroplet Impact onto a Smooth Solid Surface, *J. Appl. Fluid Mech.*, **10**, 2017, pp. 243–256.

[8] Fujimoto, H., Shiotani, Y., Tong, A.Y., Hama, T. and Takuda, H., Three-Dimensional Numerical Analysis of the Deformation Behavior of Droplets Impinging onto a Solid Substrate, *Int. J. Multiphase Flow*, **33**, 2007, pp. 317–332.

[9] Gujjula, S.R., Numerical Investigation of Droplet Spread: Effect of Contact Angle Models, *M.Sc. Thesis, U. Cincinnati*, 2015.

[10] Hirt, C.W. and Nichols, B.D., Volume of Fluid (VOF) Method for the Dynamics of Free Boundaries, *J. Comp. Phys.*, **39**, 1981, pp. 201–225.

[11] Hoang, D.A., van Steijn, V., Portela, L.M., Kreutzer, M.T. and Kleijn, C.R., Benchmark Numerical Simulations of Segmented Two-Phase Flows in Microchannels using the Volume of Fluid Method, *Computers Fluids*, **86**, 2013, pp. 28–36.

[12] Hoffman, R.L., A Study of the Advancing Interface. I. Interface Shape in Liquid-Gas Systems, *J. Colloid Interface Sci.*, **50**, 1975, pp. 228–241.

[13] Jiang, T.-S., Oh, S.-G. and Slattery, J.C., Correlation for Dynamic Contact Angle, *J. Colloid Int. Sci.*, **69**, 1979, pp. 74–77.

[14] OpenCFD, https://github.com/OpenFOAM/OpenFOAM-dev/blob/master/src/transportModels/twoPhaseProperties/alphaContactAngle/dynamicAlphaContactAngle/, viewed 2018-07-18.

[15] The OpenFOAM Foundation, OpenFOAM v5 User Guide, https://cfd.direct/openfoam/user-guide, viewed 2018-07-18.

[16] Pasandideh-Fard, M., Qiao, Y.M., Chandra, S. and Mostaghimi, J., Capillary Effects During Droplet Impact on a Solid Surface, *Phys. Fluids*, **8**, 1996, pp. 650–659.

[17] Roisman, I. V., Inertia Dominated Drop Collisions. II. An Analytical Solution of the Navier–Stokes Equations for a Spreading Viscous Film, *Phys. Fluids*, **21**, 2009, p. 052104.

[18] Scheller, B. L. and Bousfield, D. W., Newtonian Drop Impact with a Solid Surface, *AIChE J.*, **41**, 1995, pp. 1357–1367.

[19] Toivakka, M., Numerical Investigation of Droplet Impact Spreading in Spray Coating of Paper, *Proc. 8th Adv. Coating Fund. Symp.*, 2003.

[20] Voinov, O.V., Hydrodynamics of Wetting, *Fluid Dyn.*, **11**, 1976, pp 714–721.

[21] Yokoi, K., Vadillo, D., Hinch, J. and Hutchings, I., Numerical Studies of the Influence of the Dynamic Contact Angle on a Droplet Impacting on a Dry Surface, *Phys. Fluids B*, **21**, 2009, p. 072102.